nature nanotechnology

ARTICLES

PUBLISHED ONLINE: 29 AUGUST 2016 | DOI: 10.1038/NNANO.2016.159

Gapless Andreev bound states in the quantum spin Hall insulator HgTe

Erwann Bocquillon[1]*†, Russell S. Deacon[2,3]†, Jonas Wiedenmann[1]†, Philipp Leubner[1], Teunis M. Klapwijk[4], Christoph Brüne[1], Koji Ishibashi[2,3], Hartmut Buhmann[1] and Laurens W. Molenkamp[1]

In recent years, Majorana physics has attracted considerable attention because of exotic new phenomena and its prospects for fault-tolerant topological quantum computation. To this end, one needs to engineer the interplay between superconductivity and electronic properties in a topological insulator, but experimental work remains scarce and ambiguous. Here, we report experimental evidence for topological superconductivity induced in a HgTe quantum well, a 2D topological insulator that exhibits the quantum spin Hall (QSH) effect. The a.c. Josephson effect demonstrates that the supercurrent has a 4π periodicity in the superconducting phase difference, as indicated by a doubling of the voltage step for multiple Shapiro steps. In addition, this response like that of a superconducting quantum interference device to a perpendicular magnetic field shows that the 4π-periodic supercurrent originates from states located on the edges of the junction. Both features appear strongest towards the QSH regime, and thus provide evidence for induced topological superconductivity in the QSH edge states.

The realization of Majorana bound states is expected theoretically in a 1D *p*-wave superconducting phase without spin degeneracy[1,2]. A convenient experimental implementation of this exotic phase can be obtained by combining recently discovered topological states with conventional *s*-wave superconductivity[3,4]. Most of the experimental focus to date has been on 1D InAs or InSb nanowires, which may undergo a topological phase transition under an appropriate applied magnetic field. Although the first results[5,6] have been obtained, the topological origin of the observed phenomena remains unclear partly because the helical transport in the normal state has not been demonstrated. A potential alternative platform is provided by QSH insulators, in which electrons flow in two counterpropagating 1D edge states of opposite spins[7,8] (Fig. 1a). Unlike nanowires, this topological state is present in the absence of a magnetic field, and thus alleviates the requirements for high critical field superconductors[9]. Ideally, a Josephson junction formed from a QSH insulator and conventional *s*-wave superconducting contacts is expected to emulate spinless 1D *p*-wave superconductivity at its edge[10]. On each edge, it contains one Andreev doublet with a topologically protected crossing for a superconducting phase difference $\varphi = \pi$ (Fig. 1b). The two states of this gapless topological Andreev doublet (usually called Majorana bound states) have a 4π periodicity in the superconducting phase difference φ and can thus carry a 4π-periodic supercurrent, $I_{4\pi}\sin\varphi/2$, along the edges of the sample[11]. This contrasts with conventional 2π-periodic Andreev bound states that carry a current $I_{2\pi}\sin\varphi$ (+ higher harmonics). This theoretical expectation for an unconventional Josephson effect motivates our experiment.

Signatures of induced topological superconductivity

Here we report the realization of a device that follows the proposal of Fu and Kane[10] using HgTe, the first material to be identified as a topological insulator (TI)[8]. Owing to their inverted-band structure[7], HgTe quantum wells of suitable thickness are QSH insulators in which superconductivity can be induced by means of, for example, Al electrodes[12]. The anticipated presence of gapless Andreev bound states on the edges of such a device should be evidenced by two remarkable signatures, which we present as simulations in Fig. 1c,d. First, a 4π-periodic supercurrent is expected in the a.c. Josephson effect (Fig. 1c). When phase locking occurs between the junction dynamics and an external radiofrequency (RF) excitation, Shapiro steps[13] appear at discrete voltages given by $V = nhf/2e$, where n is the step index (Fig. 1c, blue line, left panel). In the presence of a 4π-periodic supercurrent, an unconventional sequence of even steps (Fig. 1c, red line, left panel) with missing odd steps is expected, which reflects the doubled periodicity of the Andreev bound states[14–16]. The exact sequence of visible steps can be highlighted by plotting a histogram of the voltage distribution as presented (Fig. 1c, right panels). In this research, we report the experimental observation of an even sequence, with missing odd steps up to $n = 9$ (Fig. 3). The estimated amplitude of the 4π-periodic supercurrent is compatible with the presence of two gapless Andreev doublets. By changing the electron density, we find that the observed effect is predominant near the expected QSH regime. In contrast, a non-topological HgTe quantum well is found with a conventional Shapiro response. Second, the response of the critical current to a perpendicular-to-plane magnetic field provides information on the spatial dependence of the current density (Fig. 1d). When a junction is dominated by planar bulk modes, the uniform flow through the plane of the quantum well results in a standard Fraunhofer pattern[17] (illustrated by a blue line in Fig. 1d). When current flows only on the edges, a d.c. superconducting quantum interference device (SQUID) response is expected[12,17] (Fig. 1d, red line). Our measurements exhibit a crossover between these two regimes, which suggests that the 4π-periodic current, indeed, flows along the edges (see Fig. 5). Additionally, in the SQUID regime, strong modulations of the odd lobes are observed, yielding an apparent doubling of the periodicity in the

[1]Physikalisches Institut (EP3), Universität Würzburg, Am Hubland, D-97074 Würzburg, Germany. [2]Advanced Device Laboratory, RIKEN, 2-1 Hirosawa, Wako-shi, Saitama, 351-0198, Japan. [3]Center for Emergent Matter Science, RIKEN, 2-1 Hirosawa, Wako-shi, Saitama, 351-0198, Japan. [4]Faculty of Applied Sciences, Kavli Institute of Nanoscience, Delft University of Technology, Lorentzweg 1, 2628 CJ Delft, The Netherlands. †These authors contributed equally to this work. *e-mail: erwann.bocquillon@physik.uni-wuerzburg.de

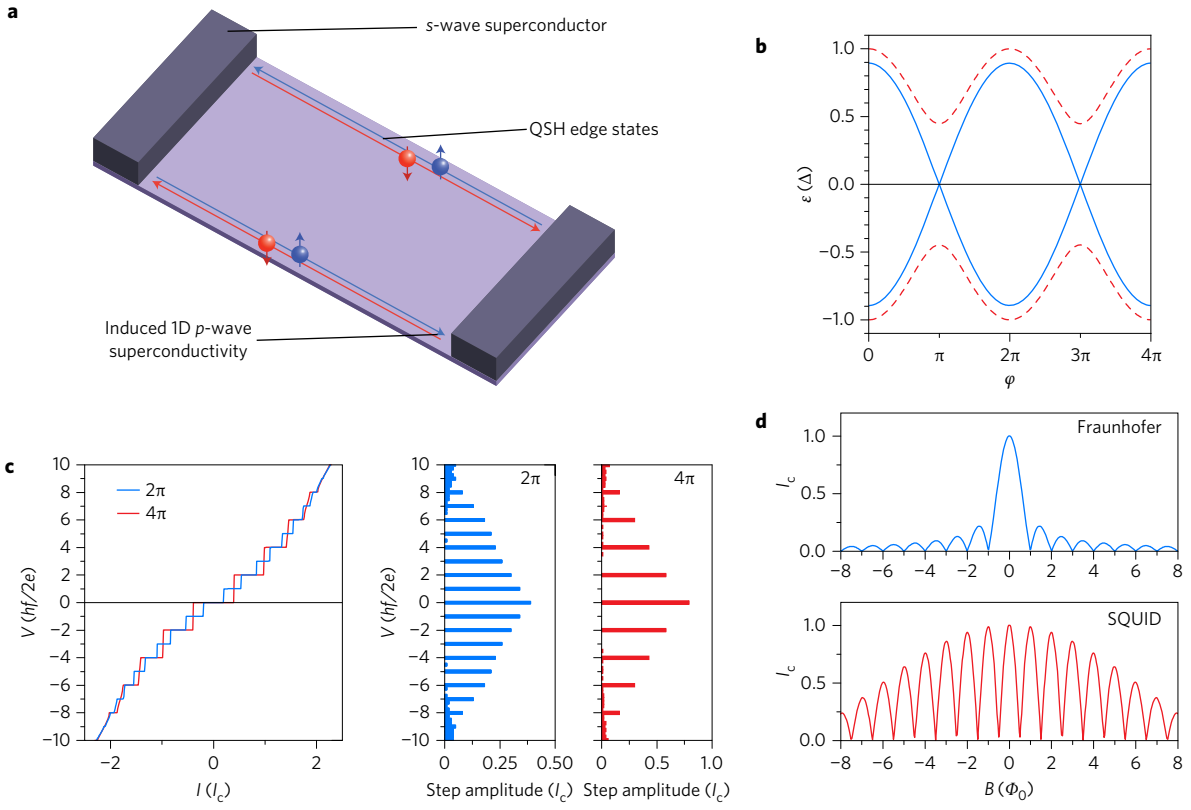

Figure 1 | Physics in a topological Josephson junction. a, Schematic of a topological Josephson junction with induced *p*-wave superconductivity. A superconducting weak link in the QSH regime contacted by two superconducting *s*-wave electrodes hosts induced *p*-wave superconductivity. **b**, Andreev spectrum of a topological *p*-wave Josephson junction (in the short junction limit). The Andreev bound states, located on the edges of the samples, have a protected crossing at zero energy ε and a 4π periodicity in the superconducting phase difference φ (blue lines), in contrast with the conventional 2π-periodic Andreev bound states (red dashed lines). **c**, Simulated d.c. current–d.c. voltage (I–V) curves in the presence of RF excitation for 2π- and 4π-periodic supercurrents, obtained with the RSJ model[32] extended to account for 4π-periodic supercurrents[28,29]. Shapiro steps of quantized voltages $V_n = nhf/2e$ (with n integer) occur in the first case, but only the sequence of even steps is visible in the latter case. Histograms of the voltage distribution (in bins of 0.25 $hf/2e$) indicate the presence of a given Shapiro step as a peak in the histogram. The two bar plots for the two curves in the left panel highlight the absence of odd steps in the case of 4π periodicity. **d**, Simulated normalized critical current I_c as a function of the magnetic field B (in units of the number of flux quanta through the junction area), following formulas in Barone and Paterno[17]. For a uniform planar current, a Fraunhofer pattern (blue line) is depicted. For current flowing on the edges, a (d.c.) SQUID pattern (red line) is expected.

magnetic flux from Φ_0 to $2\Phi_0$. Together, these sets of features strongly point towards the existence of topological gapless Andreev bound states with 4π periodicity flowing on the edges of the sample. Figure 2c summarizes the evolution of these signatures on the gate voltage axis, and we detail our experimental observations in the remainder of the article.

Properties of the Josephson junctions

The junctions are fabricated from epitaxially grown quantum wells of HgTe of thickness $d = 8$ nm, sandwiched between barrier layers of $Hg_{0.3}Cd_{0.7}Te$ on a CdZnTe substrate. In such wells (with a thickness larger than a critical thickness $d > d_c = 6.3$ nm (ref. 7)), the existence of topological edge channels in the absence of a magnetic field has been predicted and experimentally demonstrated via resistance quantization[8], non-local transport[18], spin polarization measurements[19] and scanning-SQUID imaging[20]. The layout of the Josephson junctions is presented in Fig. 2a. A rectangular mesa of HgTe sandwiched in $Hg_{0.3}Cd_{0.7}Te$ is first defined. After locally etching the cap layer, aluminium contacts are then deposited *in situ* on the HgTe layer using standard evaporation and lift-off techniques. A metallic gate (Au) is placed between the Al contacts to control the electron density. The Al superconducting contacts have a width of 1 μm. The HgTe mesa has a width of 4 μm, which corresponds to the width of the weak link. With this design, the overlap of edge channels on opposite edges is suppressed as the estimated edge channel[21,22] width is around 200 nm. The length of the junction presented in this paper is nominally $L = 400$ nm. Given an estimated mean free path $l > 2$ μm and a coherence length $\xi \approx 0.7$–2 μm, we estimate that our junction is ballistic $L < l$ and close to the short junction limit $L \leq \xi$ (see Supplementary Section I and Supplementary Fig. 1 for details).

A typical current–voltage (I–V) curve (measured at 30 mK) is presented in Fig. 2b. The junction exhibits a Josephson supercurrent with a critical current $I_c = 1.1$ μA (here for a gate voltage $V_g = 0$ V). Hysteresis is observed between forward and reverse sweeps, with a retrapping current $I_r < I_c$. For voltages larger than the energy gap of the aluminium, the I–V curve reaches an asymptote that does not go through the origin (grey line). The slope indicates the normal state resistance of the device R_n, whereas the intercept is the excess current I_{exc}. The excess current[23] stems from Andreev reflections in an energy window near the superconducting gap. It thus signals the presence of Andreev reflections at the superconductor/TI interfaces and underlines the quality of our junctions. To identify the QSH regime, it is instructive to plot the normal state resistance R_n and the critical current I_c as a function of the gate voltage V_g (Fig. 2c). We observe three regimes. For gate voltages between $V_g = -1.1$ and 0 V, R_n is low (below 300 Ω) and I_c is large (above 200 nA), which thus characterizes a high-mobility n-type

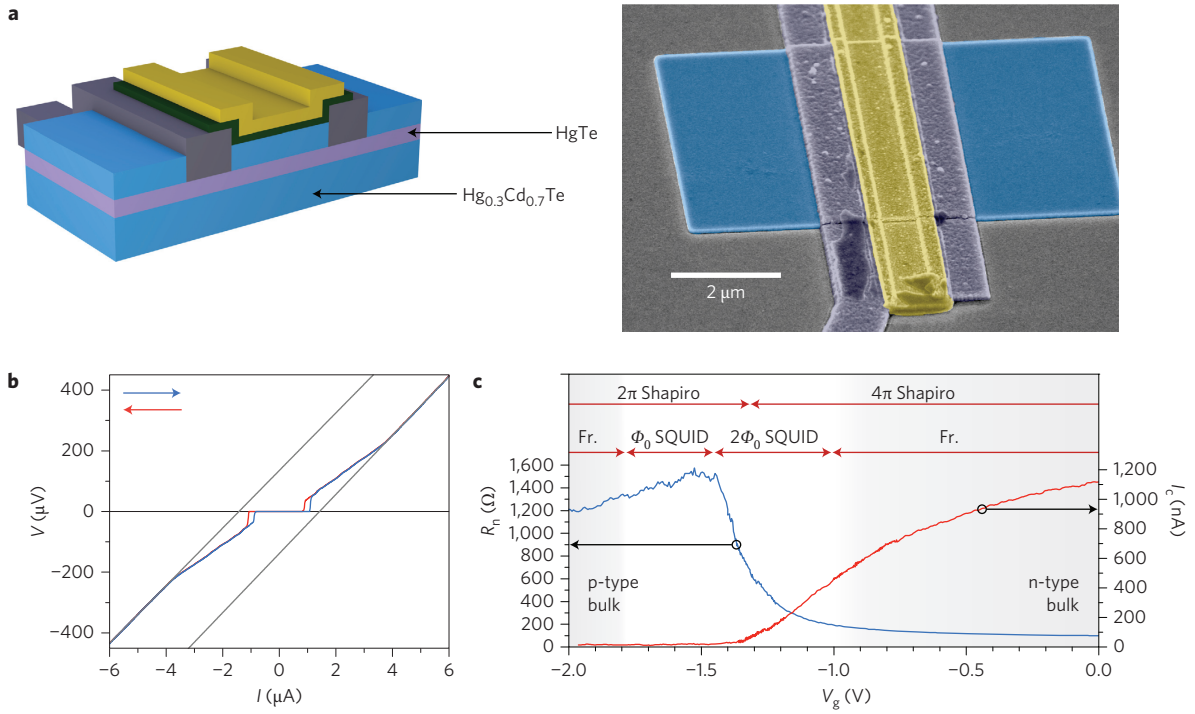

Figure 2 | Experimental realization of a topological Josephson junction. a, Artist's view and colourized scanning electron micrograph picture of a junction. The HgTe-QSH insulator (in mauve) is sandwiched between two layers of $Hg_{0.3}Cd_{0.7}Te$ (in blue). The Al superconducting contacts are in dark purple and the gate is in yellow and lies on a thin dielectric layer of HfO_2 (dark green). **b**, d.c. current–d.c. voltage (I–V) curve measured at a gate voltage of $V_g = 0$ V. This exhibits a critical current $I_c = 1.1\,\mu$A, with a weak hysteresis visible between the forward and reverse sweep (blue and red lines). For high biases, the asymptotes (grey lines) yield the normal state resistance R_n and signals the presence of an excess current I_{exc}. **c**, I_c (red line) and R_n (blue line) as a function of V_g. The red arrows summarize the ranges in which we observe the anomalous Josephson effect properties, and the grey shading indicates three different regions of gate voltage with p- and n-type bulk transport, and the expected QSH region in between. Fr., Fraunhofer.

conduction. For gate voltages below $V_g = -1.7$ V, the normal state resistance again decreases slowly, which indicates the p-conducting regime. Owing to a lower mobility in this region, the critical current I_c lies below 50 nA. In between, R_n exhibits a peak with a maximum around 1.5 kΩ (for $V_g = -1.45$ V), for which I_c is almost suppressed. This indicates the region in which the QSH edge states should be most visible. However, the peak value of R_n is lower than the expected quantized value $h/2e^2 \approx 12.9$ kΩ, which thus suggests the presence of residual bulk modes in the junction[12], possibly because of Al diffusion[24] into the HgTe material. Additionally, local n-doping caused by Al may result in p–n barriers at the interface between the Al-capped and gated areas. This would contribute to the two-point normal state resistance R_n and could obscure a correct identification of the QSH transition.

Shapiro response

The presence of gapless Andreev bound states can, in principle, be detected via the 4π-periodic contribution to the supercurrent. In practice, such detection in d.c. transport can be complicated by additional contributions from conventional 2π-periodic modes[25,26] that carry a current $I_{2\pi}\sin\varphi$ and by relaxation processes that can restore a 2π-periodic supercurrent[2,16,27]. To reveal the possible 4π-periodic characteristics, the dynamics of the junction is most conveniently probed by studying the a.c. Josephson effect. In a previous work[28], we identified anomalous features in the Shapiro response of a weak link made of the 3D TI-strained HgTe (namely, a missing first Shapiro step), which we attributed to a fractional a.c. Josephson effect consistent with the presence of a 4π-periodic Andreev doublet. Here we apply the same method to the more interesting case of a 2D TI. The I–V characteristic of the sample is measured using a d.c. current bias with the addition of an RF driving current, coupled to the device via a nearby antenna[28]. Figure 3a shows a series of histograms of the voltage distribution obtained when the excitation frequency is lowered (at $V_g = -1.1$ V; see Supplementary Fig. 2 for typical I–V curves). For a high-frequency excitation ($f = 6.6$ GHz), we observe a 'conventional' sequence of Shapiro steps at $V = nhf/2e$, $n \in Z$. As the frequency is lowered to $f = 0.8$ GHz, we observe the progressive vanishing of all the odd steps up to $n = 9$. To our knowledge, the only mechanism that results in the suppression of odd steps is the presence of a 4π-periodic contribution in the supercurrent. Although a pure 4π-periodic supercurrent should lead directly to an even sequence of Shapiro steps (as a direct effect of the substitution $\varphi \to \varphi/2$ in the Josephson equations), in our experiment it is only visible at a low frequency. Our junction may, in practice, contain both gapless bound states and a number of residual conventional modes such that the supercurrent I_s could be written as $I_s(\varphi) = I_{4\pi}\sin\varphi/2 + I_{2\pi}\sin\varphi$ (+ higher harmonics). Even in the presence of a strong 2π-periodic contribution, a 4π-periodic response can be observed when the time dependence of the voltage V to the current bias I is the most anharmonic, namely at a low frequency[28,29] (Supplementary Section II.C). Odd steps are then missing if the excitation RF, f, is lower than a frequency $f_{4\pi} = 2eR_nI_{4\pi}/h$. An estimate of the crossover frequency $f_{4\pi}$ then yields the amplitude of the 4π-periodic supercurrent $I_{4\pi}$. Estimating the crossover frequency $f_{4\pi}$ by a fully suppressed $n = 3$ step, we find that $I_{4\pi} \approx 20$ nA. The presence of two gapless Andreev bound states that carry a current of 10 nA is compatible with the maximum current $e\Delta_i/\hbar$ for the estimated induced gap $\Delta_i \approx 90$ μeV (Supplementary Fig. 1), but this estimate remains speculative, as the normal state resistance R_n is largely dominated by bulk transport in the plane, and not by edge states, which presumably carry a 4π-periodic contribution. Apart from gapless Andreev states, gapped Andreev bound states with a high transparency could also result in a 4π-periodic contribution in the

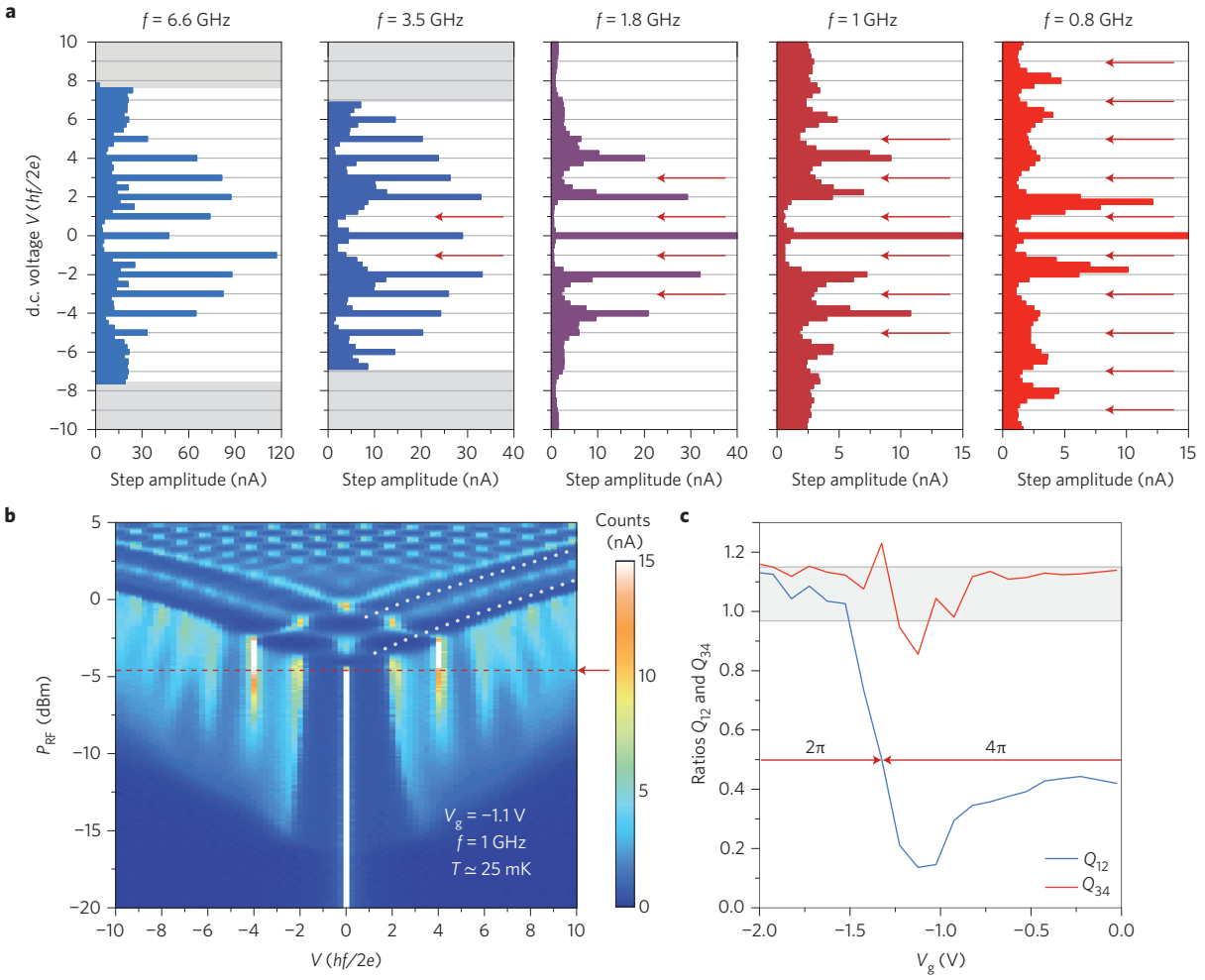

Figure 3 | Response to an RF excitation. a, Histograms of the voltage distribution obtained for different frequencies. For a high frequency, $f = 6.6$ GHz, all the steps are present. For lower frequencies, we observe the disappearance of steps $n = 1$ and 3 ($f = 1.8$ GHz) and up to $n = 9$ at $f = 0.8$ GHz. Missing steps are highlighted by red arrows. **b**, Map of the voltage distributions with voltage bins in normalized units ($hf/2e$) indicated on the abscissa and the RF excitation power P_{RF} on the ordinate. Steps $n = 1$ and 3 are completely suppressed in the low-power regime. In the oscillatory high-power regime, dark fringes (white dotted lines) develop as the first and third oscillations are suppressed. The red dashed line indicates the line cut taken in the low-power regime used to compute the histogram in **a**. **c**, Ratios of step amplitudes Q_{12} and Q_{34} measured for $f = 3.1$ GHz as a function of gate voltage V_g. Both ratios exhibit a dip in the range –1.3 to 0.9 V.

supercurrent in the presence of Landau–Zener transitions at the avoided crossing $\varphi = \pi$, 3π, … (refs 29,30). However Landau–Zener transitions have increasing probabilities with d.c. voltage or frequency. Given our observations of missing steps only at low frequencies, this possibility appears unlikely. Recently, it was proposed that Coulomb interaction and coupling of Andreev bound states to the continuum can result in a QSH system in the appearance of an 8π-periodic Josephson effect[31]. In this experimental work, we observe no sign of such an effect in the response of our devices.

We now address the dependence of the Shapiro steps on the RF power. Figure 3b shows as an example the behaviour at $f = 1.8$ GHz (see Supplementary Fig. 2 for additional data sets). A 2D map of the voltage histogram is shown as a function of voltage and excitation power P_{RF}. For low power levels, the steps progressively appear (starting from low step indices) as the power is increased. Although maxima are seen for $n = 0$, 2, 4, the first and third Shapiro steps are suppressed fully (as illustrated previously by the histogram of Fig. 3a taken along the red dashed line). As visible here, hysteresis is occasionally found to induce a weak asymmetry at low power, which affects the $n = \pm 1$ step at low frequency and low power. For high power, an oscillatory pattern (reminiscent of Bessel functions in the voltage bias case[32]) is observed. However, the pattern is deeply modified (when compared with that seen for higher-frequency excitation) with dark fringes[28] (white dotted lines), which develop from the suppression of the first and third maxima of the oscillations. In our opinion, these features signal the progressive transformation from a 2π- to a 4π-periodic pattern with halved-period oscillations that correspond to a halved number of steps.

Next, we investigate the dependence of the Shapiro response on gate voltage V_g. A general observation is that odd steps vanish at low frequencies for a very wide range of gate voltages, from about $V_g \geq -1.3$ V up to +0.5 V. The visibility of an even sequence is in agreement with the previously introduced criterion $f < f_{4\pi}$, and demonstrates that a 4π-periodic contribution is present in addition to a conventional 2π-periodic component. The latter most probably originates from bulk modes, signalling the expected coexistence of topological edge states with modes from the conduction band[33]. The 4π-periodic modes are unveiled progressively as the number of bulk modes is decreased for negative voltages. In Fig. 3c, we show a plot of the ratios Q_{12} (with respect to Q_{34}) of the maximum amplitude of the $n = 1$ to $n = 2$ steps ($n = 3$ to $n = 4$ steps, respectively) for measurements at $f = 3.1$ GHz. Simulations using the resistively shunted junction (RSJ) model[28,29] predict

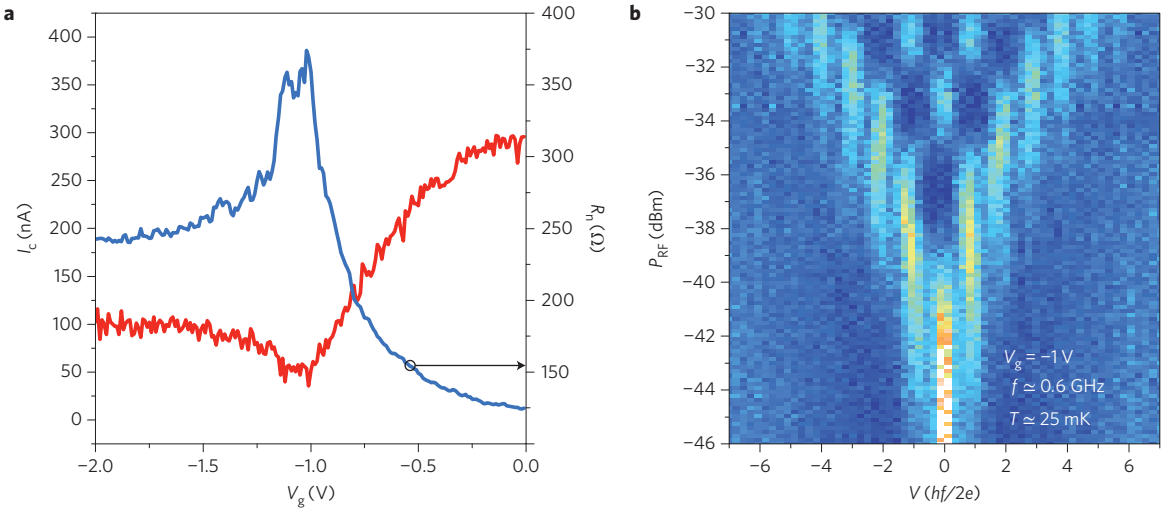

Figure 4 | Shapiro response of a junction on a trivial quantum well. a, Critical current I_c and normal state resistance R_n of a non-topological device as a function of gate voltage V_g. **b**, 2D map of the voltage distribution as a function of the d.c. voltage (in normalized units) and the RF excitation power P_{RF}, taken at $V_g \approx -1$ V and frequency $f = 0.6$ GHz. At this frequency, close to our resolution limit, all the steps are still visible.

ratios $Q_{i,i+}$, which are close to unity for a conventional junction, as indicated by the shaded grey area in Fig. 3c. Ratios that approach zero indicate the suppression and disappearance of the odd Shapiro step. Both ratios Q_{12} and Q_{34} indicate that the visibility of the even sequence of steps is improved between $V_g = 1.3$ and -0.9 V. Thus, the a.c. response of our junctions strongly signals the presence of a strong 4π-periodic contribution from the supercurrent that appears more clearly in this range close to the QSH transition. Furthermore, we emphasize that these observations are fully consistent with our previous work on the 3D TI-strained HgTe[28], in which a single gapless Andreev doublet is expected[34]. However, the observation is in this case less favourable because of the presence of a greater number of conventional modes. They displace the crossover to lower frequencies in which the visibility of the Shapiro steps is reduced, making it difficult to see more than one missing odd step. To assess the topological origin of the 4π-periodic supercurrent, we now briefly examine a narrower HgTe quantum well (thickness of $d = 5$ nm $< d_c$ (Supplementary Information)), that does not exhibit the QSH effect[8]. The measurement of the critical current I_c enables the identification of the n- and p-conduction regimes, although the gap in between, around $V_g \approx -1$ V, is not very pronounced (Fig. 4a). When measuring the Shapiro response to an RF excitation, we do not observe any missing odd step for any of the gate voltages, neither in the n- nor p-regimes, nor close to the gap. As an example, we show in Fig. 4b a measurement taken close to the gap at $V_g = -1$ V and $f = 0.6$ GHz. For such a frequency close to our detection limit, all the steps are still visible.

Response to a magnetic field

Finally, we detail the response of the junction to a magnetic field perpendicular to the plane of the junction, and show that the previous observations are compatible with edge transport in the same range. With the application of a magnetic field, the superconducting phase difference φ becomes position dependent[35]. This, in turn, reveals properties of the spatial supercurrent distribution through modulations of the critical current I_c with a period given by the magnetic flux quantum $\Phi_0 = h/2e$. In Fig. 5a, we present the differential resistance dV/dI as a function of d.c. current I and magnetic field B for different gate voltages that correspond to four different behaviours that we identify. First, for $V_g = 0$ V, the junction exhibits a conventional Fraunhofer pattern of the critical current versus magnetic field, which rapidly decays as the magnetic field increases. In this regime, the electron density is high and the current flows uniformly in the 2D plane of the quantum well. We obtain a period of circa 0.41 mT. Given the dimensions, it corresponds to an effective area of $W(L + 2\lambda) = 5.1\ \mu m^2$ and yields a penetration length $\lambda \approx 430$ nm (similar to Hart *et al.*[12]). The minima are then identified as points at which the magnetic flux Φ through the junction is a multiple of the flux quantum Φ_0 ($\Phi = n\Phi_0$, $n \in Z$). As the gate voltage is decreased, the critical current decreases and the diffraction pattern is similar to that of a (d.c.) SQUID for $V_g = -1.3$ and -1.6 V. The presence of maxima at multiples $\Phi = n\Phi_0$, $n \in Z$ is a signature of a SQUID-like behaviour and demonstrates that a sizable part of the supercurrent flows along the edges of the sample[12], as expected in the presence of QSH edge channels. In addition, the narrowing of the central lobe is clearly visible at $V_g = -1.6$ V. However, very strong odd/even modulations are observed in both cases: the first and third lobes are substantially smaller than the second and fourth. In particular, at $V_g = -1.35$ V, the first and third lobes are completely suppressed to yield an apparent doubling of the period (from Φ_0 to $2\Phi_0$) at low fields, before a conventional period is recovered for larger fields. Finally, for more-negative gate voltages ($V_g = -2$ V), the pattern progressively returns to a Fraunhofer one, with some strong distortions, especially at high fields. This suggests that the current flow returns to a 2D configuration, with inhomogeneities likely to stem from the lower mobility of the charge carriers in this gate-voltage range. In Fig. 5b, we present a 2D plot of the normalized critical current $I_c(B)/I_c(B = 0)$ when the gate voltage V_g and magnetic field B are varied. For $V_g = 0$ V to $V_g = -0.8$ V the pattern remains close to a Fraunhofer pattern, but the first and third lobes progressively disappear and are missing between -1 V and -1.5 V, as emphasized by the dotted red guides to the eye. A progressive shift of the position of the second and fourth maxima is also visible towards $\Phi/\Phi_0 \approx 2$ and 4 in the SQUID-like regime. For -1.6 V, the first and third lobes reappear. When driving the gate from $V_g = -1.6$ V to $V_g = -2$ V, a standard Fraunhofer pattern is progressively recovered.

It is tempting to associate our observations of the anomalous doubled period to a SQUID-like pattern $|\cos(\pi\Phi/2\Phi_0)|$ with periodicity $2\Phi_0$ that originates from the 4π periodicity previously identified. However, d.c. measurements are sensitive to relaxation processes that, in principle, restore a conventional Φ_0 periodicity[15,36,37], and it is unlikely that our devices are free of quasiparticle poisoning during the timescale of the experiment. Several models[38,39] have explained odd–even patterns and small deviations in a previously observed SQUID pattern[40] via skewed current-phase relations or

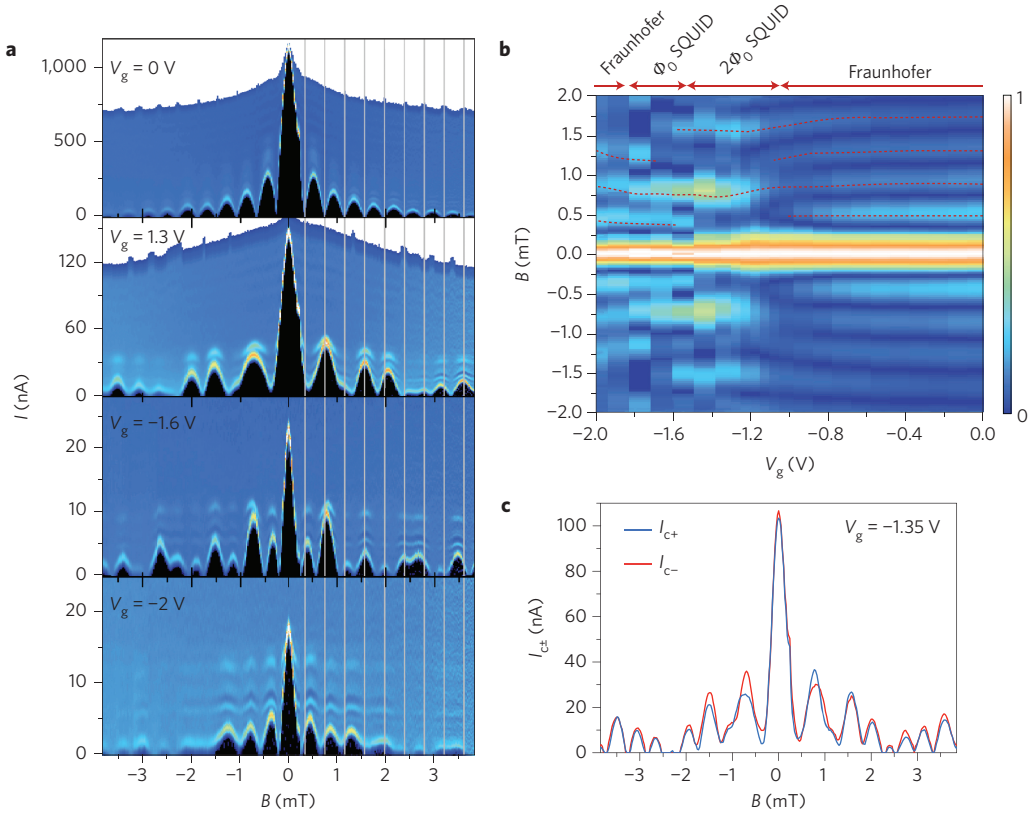

Figure 5 | Response of the critical current to a magnetic field. a, Maps of differential resistance dV/dI as a function of magnetic field B and d.c. current bias I for four different gate voltages. For V_g = 0 and −2 V, the patterns are close to the Fraunhofer diffraction ones, whereas at V_g = −1.3 and −1.6 V, a SQUID-like pattern is observed. Vertical grey lines indicate minima of the Fraunhofer pattern, where Φ is a multiple of Φ_0, that correspond to maxima of the SQUID pattern. For V_g = −1.3 V, the first and third side lobes are suppressed, which yields an apparent doubling of the period of the interference. **b**, Map of normalized critical currents I_c as a function of B and V_g. The disappearance of the first and third lobes and the shifts in the positions of the second and fourth lobes are highlighted by red dashed lines. **c**, I_c as a function of B at V_g = −1.35 V for the two sweep directions (positive as a blue line, negative as a red line), following the symmetry relation $I_{c+}(B) = I_{c-}(-B)$.

additional coupling between edges. Neither the lobe pattern nor the effect of temperature (Supplementary Fig. 4) favours such models. An alternative mechanism to explain the interference pattern is the interplay of the Zeeman effect and spin–orbit coupling, which should occur in our material system[41,42]. The interference pattern shows a peculiar symmetry relation of the critical current, $I_{c+}(B) = I_{c-}(-B)$, where + and − indicate the sweep direction of the bias current and $+B$ and $-B$ the magnetic field direction (Fig. 5c). In contrast, it is asymmetric both in the magnetic field and the sweep direction. Further investigation in a more suitable geometry is required to clarify the role of these mechanisms.

Conclusions

Finally, we return to Fig. 2c. The response to RF irradiation strongly suggests the presence of a 4π-periodic supercurrent in the device with a contribution compatible with two modes. It is most visible when the bulk bands are depleted (as indicated by the Fraunhofer interference pattern). In this region, the current flow is mostly along the edges of the sample (as indicated by the SQUID features, with possible indications of spin–orbit and Zeeman effects). Although the QSH regime is not clearly identified by its quantized conductance, it appears that the 4π-periodic contribution is also detected in the whole n-conduction band, but is rapidly suppressed when driving the gate voltage towards the p-conduction regime. This suggests that the 4π-periodic edge modes coexist in parallel with bulk modes of the conduction band, consistent with previous predictions[33] and observations in our material system[12,20]. In contrast, a Josephson junction made of a topologically trivial quantum well exhibits a conventional Shapiro response. Together, this set of observations strongly points towards the existence of the topological gapless Andreev bound states, predicted by Fu and Kane[10], in Josephson junctions produced on the well-characterized QSH insulator HgTe. Although further developments are required to comprehend fully the richness of the observed phenomena, Josephson junctions in HgTe quantum wells and at zero magnetic field appear promising for the future realization of Majorana end states and possibly scalable Majorana qubits.

Received 29 January 2016; accepted 21 July 2016;
published online 29 August 2016

References

1. Kitaev, A. Unpaired Majorana fermions in quantum wires. *Phys. Usp.* **44,** 16 (2001).
2. Kwon, H. J., Yakovenko, V. M. & Sengupta, K. Fractional a.c. Josephson effect in unconventional superconductors. *Low Temp. Phys.* **30,** 613–619 (2004).
3. Alicea, J. New directions in the pursuit of Majorana fermions in solid state systems. *Rep. Prog. Phys.* **75,** 076501 (2012).
4. Beenakker, C. W. J. Search for Majorana fermions in superconductors. *Annu. Rev. Cond. Mat. Phys.* **4,** 113–136 (2013).
5. Mourik, V. *et al.* Signatures of Majorana fermions in hybrid superconductor–semiconductor nanowire devices. *Science* **336,** 1003–1007 (2012).
6. Rokhinson, L. P., Liu, X. & Furdyna, J. K. The fractional a.c. Josephson effect in a semiconductor/superconductor nanowire as a signature of Majorana particles. *Nat. Phys.* **8,** 795–799 (2012).
7. Bernevig, B. A., Hughes, T. L. & Zhang, S.-C. Quantum spin Hall effect and topological phase transition in HgTe quantum wells. *Science* **314,** 1757–1761 (2006).
8. König, M. *et al.* Quantum spin Hall insulator state in HgTe quantum wells. *Science* **318,** 766 (2007).

9. Samkharadze, N. *et al.* High kinetic inductance superconducting nanowire resonators for circuit QED in a magnetic field. *Phys. Rev. Applied* **5,** 044004 (2016).
10. Fu, L. & Kane, C. L. Josephson current and noise at a superconductor/quantum-spin-Hall-insulator/superconductor junction. *Phys. Rev. B* **79,** 161408 (2009).
11. Beenakker, C. W. J. *et al.* Fermion-parity anomaly of the critical supercurrent in the quantum spin-Hall effect. *Phys. Rev. Lett.* **110,** 017003 (2013).
12. Hart, S. *et al.* Induced superconductivity in the quantum spin Hall edge. *Nat. Phys.* **10,** 638–643 (2014).
13. Shapiro, S. Josephson currents in superconducting tunneling: the effect of microwaves and other observations. *Phys. Rev. Lett.* **11,** 80–82 (1963).
14. San-Jose, P., Prada, E. & Aguado, R. AC Josephson effect in finite-length nanowire junctions with Majorana modes. *Phys. Rev. Lett.* **108,** 257001 (2012).
15. Houzet, M., Meyer, J. S., Badiane, D. M. & Glazman, L. I. Dynamics of Majorana states in a topological Josephson junction. *Phys. Rev. Lett.* **111,** 046401 (2013).
16. Badiane, D. M., Glazman, L. I., Houzet, M. & Meyer, J. S. AC Josephson effect in topological Josephson junctions. *C. R. Phys.* **14,** 840–856 (2013).
17. Barone, A. & Paterno, G. *Physics and Applications of the Josephson Effect* (Wiley and Sons, 1982).
18. Roth, A. *et al.* Nonlocal transport in the quantum spin Hall state. *Science* **325,** 294–297 (2009).
19. Brüne, C. *et al.* Spin polarization of the quantum spin Hall edge states. *Nat. Phys.* **8,** 485–490 (2012).
20. Nowack, K. C. *et al.* Imaging currents in HgTe quantum wells in the quantum spin Hall regime. *Nat. Mater.* **12,** 787–791 (2013).
21. Zhou, B. *et al.* Finite size effects on helical edge states in a quantum spin-Hall system. *Phys. Rev. Lett.* **101,** 246807 (2008).
22. Brüne, C. *et al.* Evidence for the ballistic intrinsic spin Hall effect in HgTe nanostructures. *Nat. Phys.* **6,** 448–454 (2010).
23. Blonder, G. E., Tinkham, M. & Klapwijk, T. M. Transition from metallic to tunneling regimes in superconducting microconstrictions: excess current, charge imbalance, and supercurrent conversion. *Phys. Rev. B* **25,** 4515–4532 (1982).
24. Capper, P. *Properties of Narrow Gap Cadmium-Based Compounds* (Inspec, 1994).
25. Finck, A. D. K., Kurter, C., Hor, Y. S. & Van Harlingen, D. J. Phase coherence and Andreev reflection in topological insulator devices. *Phys. Rev. X* **4,** 041022 (2014).
26. Galletti, L. *et al.* Influence of topological edge states on the properties of Bi_2Se_3/Al hybrid Josephson devices. *Phys. Rev. B* **89,** 134512 (2014).
27. Pikulin, D. I. & Nazarov, Y. V. Phenomenology and dynamics of a Majorana Josephson junction. *Phys. Rev. B* **86,** 140504 (2012).
28. Wiedenmann, J. *et al.* 4π-periodic Josephson supercurrent in HgTe-based topological Josephson junctions. *Nat. Commun.* **7,** 10303 (2016).
29. Domínguez, F., Hassler, F. & Platero, G. Dynamical detection of Majorana fermions in current-biased nanowires. *Phys. Rev. B* **86,** 140503 (2012).
30. Sau, J. D., Berg, E. & Halperin, B. I. On the possibility of the fractional a.c. Josephson effect in non-topological conventional superconductor–normal–superconductor junctions. Preprint at http://arxiv.org/abs/1206.4596 (2012).
31. Zhang, F. & Kane, C. L. Time-reversal-invariant Z_4 fractional Josephson effect. *Phys. Rev. Lett.* **113,** 036401 (2014).
32. Russer, P. Influence of microwave radiation on current–voltage characteristic of superconducting weak links. *J. Appl. Phys.* **43,** 2008 (1972).
33. Dai, X. *et al.* Helical edge and surface states in HgTe quantum wells and bulk insulators. *Phys. Rev. B* **77,** 125319 (2008).
34. Tkachov, G. & Hankiewicz, E. M. Helical Andreev bound states and superconducting Klein tunneling in topological insulator Josephson junctions. *Phys. Rev. B* **88,** 075401 (2013).
35. Tinkham, M. *Introduction to Superconductivity* (Dover, 2004).
36. Fu, L. & Kane, C. L. Superconducting proximity effect and Majorana fermions at the surface of a topological insulator. *Phys. Rev. Lett.* **100,** 096407 (2008).
37. Lee, S.-P., Michaeli, K., Alicea, J. & Yacoby, A. Revealing topological superconductivity in extended quantum spin Hall Josephson junctions. *Phys. Rev. Lett.* **113,** 197001 (2014).
38. Baxevanis, B., Ostroukh, V. P. & Beenakker, C. W. J. Even–odd flux quanta effect in the Fraunhofer oscillations of an edge-channel Josephson junction. *Phys. Rev. B* **91,** 041409 (2015).
39. Tkachov, G., Burset, P., Trauzettel, B. & Hankiewicz, E. M. Quantum interference of edge supercurrents in a two-dimensional topological insulator. *Phys. Rev. B* **92,** 045408 (2015).
40. Pribiag, V. S. *et al.* Edge-mode superconductivity in a two-dimensional topological insulator. *Nat. Nanotech.* **10,** 593–597 (2015).
41. Dolcini, F., Houzet, M. & Meyer, J. S. Topological Josephson φ_0 junctions. *Phys. Rev. B* **92,** 035428 (2015).
42. Rasmussen, A. *et al.* Effects of spin–orbit coupling and spatial symmetries on the Fraunhofer interference pattern in SNS junctions. *Phys. Rev. B* **93,** 155406 (2016).

Acknowledgements

We thank V. Hock and L. Maier for technical assistance and acknowledge S. Tarucha, L. Glazman, Y. Peng, F. von Oppen, E.M. Hankiewicz, G. Tkachov and B. Trauzettel for enlightening discussions. This work is supported by the German Research Foundation (Leibniz Program, DFG-Sonderforschungsbereich 1170 'Tocotronics' and DFG-Schwerpunktprogramme 1666), the Elitenetzwerk Bayern program Topologische Isolatoren. R.S.D. acknowledges support from Grants-in-Aid for Scientific Research A (No. 16H02204) and Young Scientists B (No. 26790008). T.M.K. is financially supported by the European Research Council Advanced Grant No.339306 (METIQUM). E.B., T.M.K. and L.W.M. thank the Alexander von Humboldt foundation for its support.

Author contributions

E.B., R.S.D., J.W., T.M.K., K.I., C.B., H.B. and L.W.M. conceived the experiments. P.L. and C.B. grew the material, and contributed material analysis. J.W. prepared the samples, with inputs from E.B., and R.S.D. E.B. and J.W. performed the measurements and the analysis. All the authors contributed to analysing and interpreting the data, and to writing the manuscript.

Additional information

Supplementary information is available in the online version of the paper. Reprints and permissions information is available online at www.nature.com/reprints. Correspondence and requests for materials should be addressed to E.B.

Competing financial interests

The authors declare no competing financial interests.